

Modelling the sources of the pulse artefact in simultaneous EEG/fMRI

W. X. Yan¹, K. J. Mullinger¹, G. B. Geirsdottir¹, and R. W. Bowtell¹

¹Sir Peter Mansfield Magnetic Resonance Center, School of Physics and Astronomy, University of Nottingham, Nottingham, Nottinghamshire, United Kingdom

Introduction

Simultaneous electroencephalography (EEG) and functional magnetic resonance imaging (fMRI) is hindered by the generation of large artefacts in the EEG recordings. The pulse artefact (PA) is particularly challenging because of its persistence even after application of artefact correction algorithms (1-3). Several different causes of the PA have been proposed (1, 4-6), but few studies have analysed their relative importance. Here we present analytic expressions and simulations developed from basic physical principles describing two possible causes of the PA: cardiac-pulse-induced head rotation and Hall voltages generated by blood flow. Through physical modelling we determine whether these mechanisms are realistic causes of the PA, and compare the results of calculations with experimental measurements.

Theory and Methods

Rotation: We model the head as a uniform, spherical volume conductor and consider two contributions to the artefact voltage:

(i) the voltage induced in the moving conductive EEG leads; (ii) the scalar potential, Φ , resulting from the magnetic force acting on moving charges in the volume conductor. Our model assumes that the EEG leads run along the meridians of the sphere, coming together in a cable bundle at its north pole. The total potential difference produced at the amplifier inputs from leads connected to a 'data' electrode at point 'A' and a 'reference' electrode at point 'C' on the head is then described by Eq. [1], where the two leads join the cable bundle at position 'B', \mathbf{v} is the local velocity in the frame where the static magnetic field, \mathbf{B} , is fixed and $d\mathbf{l}$ characterises an infinitesimal section of the lead. Evaluation of this expression shows that in a uniform field, translational motion induces no artefact voltages, whereas voltages are generated by a rotation about an axis perpendicular to \mathbf{B} : head rotation driven by cardiac pulsation could thus cause the PA.

Blood flow: The ions in a conducting fluid, such as blood, experience a force when the fluid flows in a magnetic field. As a result a charge distribution builds up at the vessel wall, which generates an electric field that causes current flow in conducting tissue surrounding the vessel. Pulsatile flow thus produces a temporally varying voltage at the surface of the body, which could cause the PA. Here, we modelled a blood vessel as a cylinder of radius, b , and length, L ($\gg b$), carrying blood flowing at a velocity, \mathbf{v} , in an applied magnetic field, \mathbf{B} . When this vessel is embedded in a conducting medium, its effect can be modelled as that of a current dipole, \mathbf{Q} , oriented perpendicular to \mathbf{v} and \mathbf{B} as described by Eq. [3], where σ is the conductivity of the medium.

Experimental: Recordings were made inside a Philips Achieva 3T MR system using BrainAmp MR-plus EEG amplifiers (Brain Products). Electrode positions were recorded using a Polhemus Isotrack system to allow comparison with the results of modelling based on the best-fitting sphere to the phantom or head. EEG data were first recorded from a healthy volunteer lying in a supine position, with his head centred in the bore of the 3 T magnet. After the intrinsic PA had been recorded, additional measurements were made while the subject nodded his head slowly. To further assess the effect of rotation, a 32-electrode EEG cap was placed on a 19 cm diameter, spherical, conducting agar phantom (7) which was then positioned in the bore of the MR scanner atop a roller platform which rotated the phantom about its x -axis at $\sim 30^\circ \text{ s}^{-1}$. A similar phantom containing a 1cm diameter flow channel was used with a 64-electrode EEG cap to measure the effect of flow. Saline solution was pulsed at a velocity of $\sim 20 \text{ cm s}^{-1}$ through the channel in the anterior to posterior direction.

Results

The measured PA showed two distinct peaks delayed by times of $\sim 170 \text{ ms}$ and $\sim 260 \text{ ms}$ relative to the R-peak. Figure 1 shows artefact maps recorded at the two peaks, indicating a predominantly left-right variation of voltage with a reversal of polarity of the second smaller peak compared with the first, as previously described (6).

Rotation: Figure 2A shows the artefact pattern produced by simulation of a nodding motion. This is very similar in spatial form to the measured PA, and is described by Eq. [2] where B_θ is the static field, a is the radius of the sphere, Ω is the angular velocity about the x -axis (+ve = nod forward), ϕ_E and θ_E describe the position of the electrode and α characterises the instantaneous angle of rotation of the head. Figure 2B shows the voltages measured on the rotating phantom, confirming that a nodding motion produces a voltage pattern that is very similar to the measured PA. A similar pattern was produced when the subject nodded his head. Calculating the correlation of measured and simulated artefact voltages for the rotating phantom gave a correlation coefficient (CC) of 0.98. Comparison of the voltage pattern calculated for head rotation and the measured PA gave a highly significant CC of 0.87. Fitting Eq. [2] to the measured PA indicates that angular velocities of just $-0.46^\circ \text{ s}^{-1} / +0.49^\circ \text{ s}^{-1}$ are needed to produce the voltages measured at the temporal peaks of the PA. Subtraction of simulated data from the measured PA reduced the voltage variance measured across electrodes to 34 % of its original value.

Blood flow: Equation [3] implies that large arteries in which blood flows rapidly and perpendicular to the applied field will produce the largest effects. The form of the artefact voltage produced on the scalp depends on the position and orientation of the effective dipole inside the head. Based on the spatial form of the PA and the anatomical location of large arteries, we considered the situation where the dipole is located at the centre of the head, which is modelled again as a sphere. In these circumstances it can be shown (8) that the voltage generated at position, \mathbf{r} , on the surface of the sphere is given by Eq. [4]. With the flow directed posterior-to-anterior, the potential thus varies linearly with x -coordinate, producing a characteristic left-right polarity variation as seen in the PA. This is confirmed by Fig. 3, which shows the potentials measured on the flow phantom. Inserting realistic parameters for blood flow in large cerebral arteries ($b = 0.5 \text{ cm}$, $L = 1 \text{ cm}$, $|\mathbf{v}| = 13 \text{ cm s}^{-1}$) into Eqs. [3&4] yields a dipole strength of 15 nA m^1 and peak voltages at the surface of the sphere of just $\pm 8 \mu \text{ V}$ at 3T.

Discussion and Conclusions

The strong similarity of the measured PA and the voltages generated by head rotation about the x -axis indicate that a nodding motion driven by cardiac pulsation is a plausible source of the PA. The calculations indicate that the measured voltages could be generated by realistic angular velocities – summing over the PA waveform we estimate that angular excursions of less than $\pm 0.1^\circ$ would be needed to explain the measured voltages. Analysis of the PA polarity suggests that the head first nods backward when the rapid blood flow from the carotid and vestibular arteries is redirected into smaller arteries in the head (1st peak of PA), followed by a second restorative motion corresponding to a forward nod (2nd peak). The morphology of the potentials due to blood flow derived from Eqs. [3&4] also correlates highly with the measured PA. However, the Hall voltage magnitudes calculated for typical anatomical parameters are more than 20 times smaller than those measured in the PA and the presence of the low conductivity skull layer in a head would considerably reduce these voltages further. We therefore conclude that the predominant cause of the PA is a nodding motion, although other factors such as blood flow in superficial vessels and scalp expansion may also contribute. Development of a deeper understanding of the PA, as described here, is a key step in working towards production of higher fidelity EEG/fMRI data (9): analytic expressions can guide the redesign of wiring layouts on EEG caps so as to minimise intrinsic artefact pickup, while simulated artefact maps could be incorporated into selective filters to improve analysis methods.

References [1] Allen *et al* Neuroimage 8:229,1998, [2] Debener *et al* Neuroimage, 34:587, 2007 [3] Naizy *et al* Neuroimage 28:720, 2005 [4] Bonmassar *et al* Neuroimage 16:1127, 2002 [5] Nakamura *et al* IEEE Trans Biomed. Eng. 53:1294, 2006 [6] Debener *et al*. Int. J. Psychophysiol. 67:189, 2008 [7] Yan *et al*, Neuroimage, 46:459, 2009; [8] Yao *et al* IEEE Trans Biomed. Eng 47:964, 2000 [9] Yan *et al*, HBM, (in press)

$$V = \Phi_A - \Phi_C - \int_B^A \mathbf{v} \times \mathbf{B} \cdot d\mathbf{l} + \int_B^C \mathbf{v} \times \mathbf{B} \cdot d\mathbf{l} \quad [1]$$

$$V = \frac{a^2 B_\theta \Omega \cos \alpha}{2} \theta_E \cos \phi_E \quad [2]$$

$$Q = \sigma \pi b^2 L (\mathbf{v} \times \mathbf{B}) \quad [3]$$

$$V = \frac{3b^2 L}{4a^3} (\mathbf{v} \times \mathbf{B}) \cdot \mathbf{r} \quad [4]$$

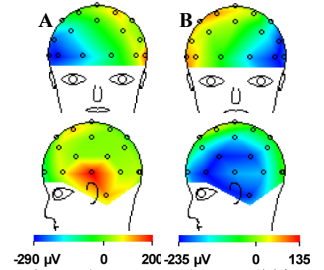


Figure 1: In vivo PA maps A) 1st peak; B) 2nd peak.

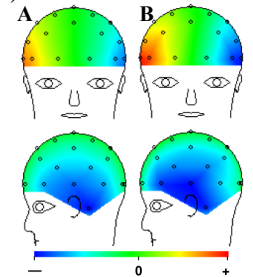


Figure 2: Showing A) simulated; B) experimental results on the phantom for + x -axis rotation.

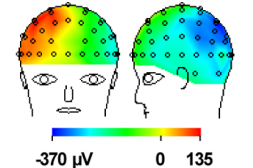


Figure 3: Flow artefact recorded on phantom